Nucleic Acids Research, 2006, Vol. 34, No. 8 ***2305–2315***
doi:10.1093/nar/gkl099

Genetic effects of oxidative DNA damages: comparative mutagenesis of the imidazole ring-opened formamidopyrimidines (Fapy lesions) and 8-oxo-purines in simian kidney cells

M. Abul Kalam, Kazuhiro Haraguchi[1], Sushil Chandani[2], Edward L. Loechler[2], Maasaki Moriya[3], Marc M. Greenberg[1] and Ashis K. Basu*

Department of Chemistry, University of Connecticut, Storrs, CT 06269, USA, [1]Department of Chemistry, Johns Hopkins University, Baltimore, MD 21218, USA, [2]Biology Department, Boston University, Boston, MA 02118, USA and [3]Department of Pharmacological Sciences, State University of New York, Stony Brook, NY 11794, USA

Received December 1, 2005; Revised January 9, 2006; Accepted March 7, 2006

ABSTRACT

Fapy·dG and 8-oxo-7,8-dihydro-2′-deoxyguanosine (8-oxo-dG) are formed in DNA by hydroxyl radical damage. In order to study replication past these lesions in cells, we constructed a single-stranded shuttle vector containing the lesion in 5′-TGT and 5′-TGA sequence contexts. Replication of the modified vector in simian kidney (COS-7) cells showed that Fapy·dG is mutagenic inducing primarily targeted Fapy·G→T transversions. In the 5′-TGT sequence mutational frequency of Fapy·dG was ∼30%, whereas in the 5′-TGA sequence it was ∼8%. In parallel studies 8-oxo-dG was found to be slightly less mutagenic than Fapy·dG, though it also exhibited a similar context effect: 4-fold G→T transversions (24% versus 6%) occurred in the 5′-TGT sequence relative to 5′-TGA. To investigate a possible structural basis for the higher G→T mutations induced by both lesions when their 3′ neighbor was T, we carried out a molecular modeling investigation in the active site of DNA polymerase β, which is known to incorporate both dCTP (no mutation) and dATP (G→T substitution) opposite 8-oxo-G. In pol β, the *syn*-8-oxo-G:dATP pair showed greater stacking with the 3′-T:A base pair in the 5′-TGT sequence compared with the 3′-A:T in the 5′-TGA sequence, whereas stacking for the *anti*-8-oxo-G:dCTP pair was similar in both 5′-TGT and 5′-TGA sequences. Similarly, *syn*-Fapy·G:dATP pairing showed greater stacking in the 5′-TGT sequence compared with the 5′-TGA sequence, while stacking for *anti*-Fapy·G:dCTP pairs was similar in the two sequences. Thus, for both lesions less efficient base stacking between the lesion:dATP pair and the 3′-A:T base pair in the 5′-TGA sequence might cause lower G→T mutational frequencies in the 5′-TGA sequence compared to 5′-TGT. The corresponding lesions derived from 2′-deoxyadenosine, Fapy·dA and 8-oxo-dA, were not detectably mutagenic in the 5′-T*A*T sequence, and were only weakly mutagenic (<1%) in the 5′-T*A*A sequence context, where both lesions induced targeted A→C transversions. To our knowledge this is the first investigation using extrachromosomal probes containing a Fapy·dG or Fapy·dA site-specifically incorporated, which showed unequivocally that in simian kidney cells Fapy·G→T substitutions occur at a higher frequency than 8-oxo-G→T and that Fapy·dA is very weakly mutagenic, as is 8-oxo-dA.

INTRODUCTION

The accumulation of oxidative damages in DNA is believed to play a role in aging and various diseases (1–3). Ionizing radiation generates many of the same lesions in DNA that are formed by oxidative stress (4,5). A ubiquitous product of ionizing radiation and oxidation is 8-oxo-7,8-dihydro-2′-deoxyguanosine (8-oxo-dG) that has received much attention since the late 1980s (6–8). A major fraction of 8-oxo-dG is believed to be formed by hydroxyl radical damage, which also generates Fapy·dG [*N*-(2-deoxy-D-pentofuranosyl)-*N*-(2,6-diamino-4-hydroxy-5-formamidopyrimidine)], presumably via a common radical intermediate (Scheme 1) (9,10).

*To whom correspondence should be addressed. Tel: +1 860 486 3965; Fax: +1 860 486 2981; Email: ashis.basu@uconn.edu

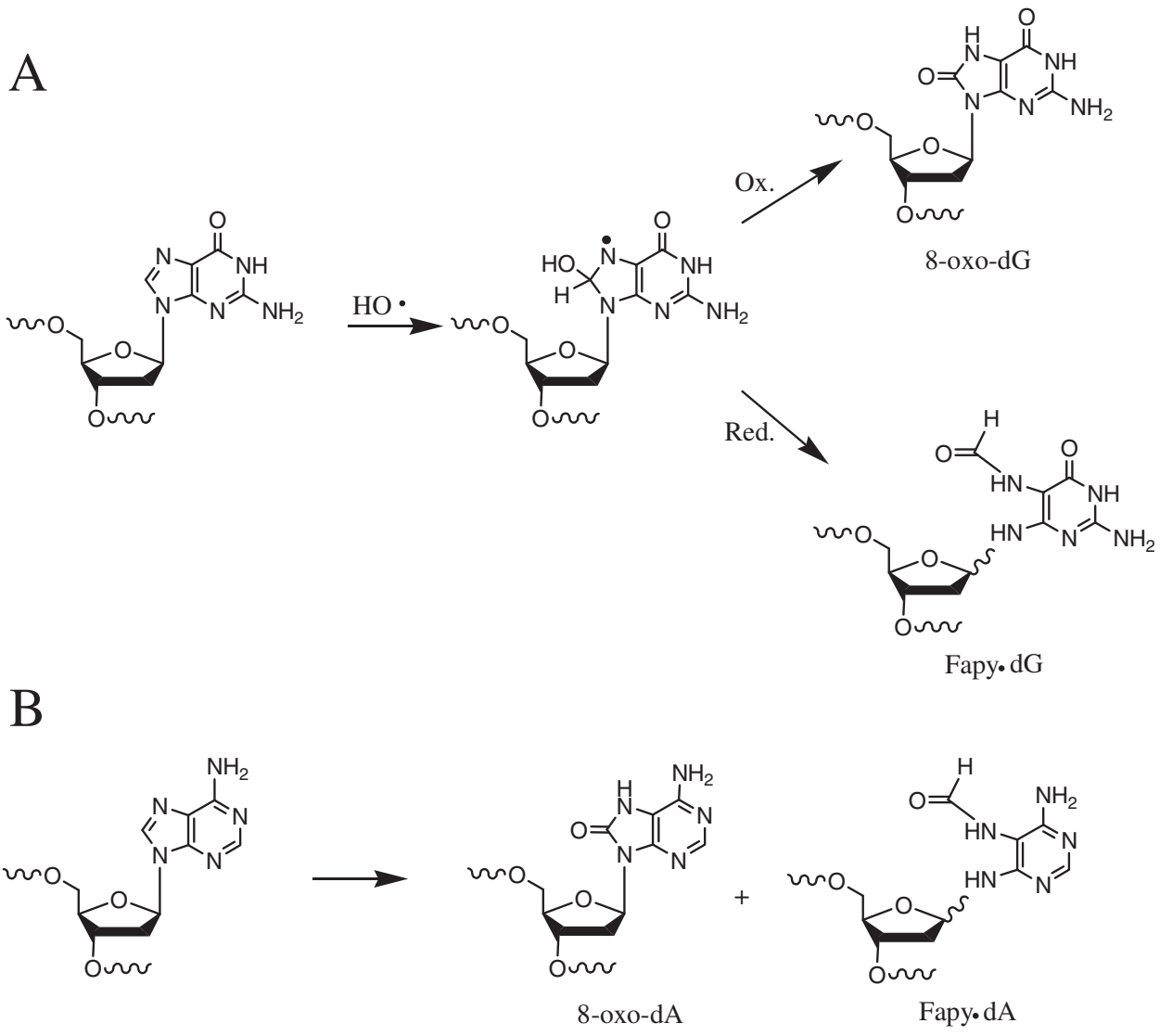

Scheme 1. (**A** and **B**) Postulated hydroxyl radical mediated pathway to Fapy·dG, 8-oxo-dG and Fapy·dA, 8-oxo-dA.

Fapy·dG is a more common DNA lesion under reductive conditions and during exposure to UV light (11,12), but few studies have been performed on its biological effects. Fapy·dG is subject to excision by repair enzymes of which one, formamidopyrimidine glycosylase (fpg, MutM), formally bears its name, even though it is known to excise several oxidative damages (13). Similar to the situation with dG, oxidative insult to DNA generates Fapy·dA and 8-oxo-dA from a common intermediate, and oxygen-deficient conditions gives rise to higher level of Fapy·dA than 8-oxo-dA (14,15). However, in aqueous solution DNA exposed to γ-radiolysis generates Fapy·dA 10-fold less efficiently than it does Fapy·dG (16).

Recent advances in the synthesis of oligonucleotides containing Fapy·dG (17,18) and Fapy·dA (19) provide the tool which are required in order to carry out repair and replication studies on biopolymers containing these lesions incorporated at defined sites. *In vitro* replication studies using Klenow exo$^-$ fragment from DNA polymerase I of *Escherichia coli* show that Fapy·dG is efficiently bypassed and that dA is misincorporated opposite it (20). Likewise, Fapy·dA induces nucleotide misincorporation *in vitro*, albeit infrequently (21). Repair studies show that Fapy·dG opposite dC is excised by fpg much more efficiently than when it is mispaired with dA (22).

The results of these replication and repair studies suggest that both Fapy·dG and Fapy·dA have the potential to be mutagenic in cells. In order to unambiguously address this, in the current work we evaluated the mutagenic potential of Fapy·dG and Fapy·dA in mammalian cells using a shuttle phagemid vector. We also compared the mutational types and frequencies of the Fapy lesions with the corresponding 8-oxo-purines. In addition, molecular modeling studies were carried out in order to rationalize the observed sequence context effects on replication of the Fapy- and 8-oxo-purine lesions in cells.

MATERIALS AND METHODS

Materials

[γ-^{32}P]ATP was from Du Pont New England Nuclear (Boston, MA). T4 DNA ligase and T4 polynucleotide kinase were

obtained from New England Biolabs (Beverly, MA). *E.coli* strain DH10B was purchased from Gibco BRL and COS-7 cells are available in our laboratory. Single-stranded phagemid, pMS2, DNA was prepared from *E.coli* JM109 with the aid of the helper phageVCSM13 (Stratagene, La Jolla, CA) as reported by Moriya (23).

Methods

Synthesis and characterization of oligonucleotides. The synthesis and characterization of Fapy·dG dodecamers, d(TGC AGT XTC AGC) and d(TGC AGT XAC AGC) (where X = Fapy·dG) (17) and Fapy·dA dodecamers d(TGC ACT XAC AGC) and d(TGC ACT XTC AGC) (where X = Fapy·dA) (19) have been reported. 8-Oxo-dG, 8-oxo-dA and control oligonucleotides of the corresponding sequences were synthesized by the Midland Certified Reagent Company, Inc (Midland, TX). The 8-oxo-dG and 8-oxo-dA oligonucleotides were deprotected with concentrated NH_4OH for 18 h at 55°C in the presence of 0.25 M β-mercaptoethanol and purified by C18 reverse phase high-performance liquid chromatography followed by denaturing PAGE. Mass spectrometric analysis by MALDI-TOF verified the molecular weight of the oligonucleotides.

Construction and characterization of pMS2 vectors containing a single Fapy·dG, 8-oxo-dG, Fapy·dA or 8-oxo-dA. The single-stranded pMS2 shuttle vector, which contains its only EcoRV site in a hairpin region, was prepared as described elsewhere (23,24). The pMS2 DNA (58 pmol, 100 μg) was digested with a large excess of EcoRV (300 pmol, 4.84 μg) for 1 h at 37°C followed by room temperature overnight. A 58mer scaffold oligonucleotide (containing a T opposite the potential lesion site) was annealed overnight at 9°C to form the gapped DNA. The control and lesion containing 12mers were phosphorylated with T4 polynucleotide kinase, hybridized to the gapped pMS2 DNA, and ligated overnight at 16°C. Unligated oligonucleotides were removed by passing through Centricon-100 and the DNA was precipitated with ethanol. The scaffold oligonucleotide was digested by treatment with T4 DNA polymerase and exonuclease III, the proteins were extracted with phenol/chloroform, and the DNA was precipitated with ethanol. The final construct was dissolved in 1 mM Tris–HCl, 0.1 mM EDTA, pH 8, and a portion was subjected to electrophoresis on 1% agarose gel in order to assess the amount of circular DNA.

Replication and analysis in simian kidney cells. COS-7 cells were grown in DMEM supplemented with 10% fetal bovine serum. The cells were seeded at 5×10^5 cells per 60 mm plate. Following overnight incubation, the cells were transfected with 50 ng of single-stranded DNA (ssDNA) by electroporation. The culture was incubated for 2 days, and the progeny plasmid was recovered by the method of Hirt (25). It was then used to transform *E.coli* DH10B, and transformants were analyzed by oligonucleotide hybridization (26). In some of the experiments an AA mismatch three nucleotides 5′ to the lesion (or a control G or A) was introduced to estimate the extent of scaffold removal. Based on the number of transformants that contained a T 3 nt 5′ to the lesion (<1%) and/or an A at the lesion site (none recovered) due to mismatch repair, we believe that the scaffold removal was nearly quantitative in these experiments.

Molecular mechanics calculations. Structures were constructed, viewed, manipulated and analyzed using Insight II (Molecular Simulations, Inc. version 98.0) (27). Visualizations and calculations were conducted on an SGI O2, SGI Origin 200 and an IBM pSeries 690. The CHARMM 27 all-atom forcefield (28,29) was used to calculate energies and direct all minimizations and molecular dynamics (MD) calculations. Parameters for 8-oxo-G and Fapy·G are given in Supplementary Data. Preliminary minimizations followed previously established protocols (30), and, when needed, *de novo* DNA coordinates were generated from canonical fiber diffraction B-DNA (31). Structures with 8-oxo-G were compared with NMR and X-ray structures (32,33).

Fapy·G can exist in several conformers via rotations about the C5-N7 and N7-C8 bonds. Calculations were conducted on the rotational conformer that resembles guanine itself, which has C8H/N9H eclipsing, as well as the rotational isomer with C8O/N9H eclipsing, because these conformations were observed in a solution study of a Fapy·dG derivative, and they were of approximately the same energy (34). Both eclipsing orientations were explored, but each one yielded the same final orientation in minimization studies (Supplementary Data), where the eclipsing C8H (or the C8O in the other rotamer) lies to the 5′-side with HN9 to the 3′-side.

The algorithm '3DNA' was used to calculate the amount of overlap between adjacent, stacked base pairs in Angstroms squared ($Å^2$) (35). Overlap areas for both all-atoms and endocyclic (aromatic) atoms only are reported. Each structure was rigorously examined, and during this process we discovered that 3DNA viewed the Fapy·dG ring-opened formamido region to be ring-closed, since the computed overlap areas involving the endocyclic atoms of Fapy·dG did not correspond well with the structure. This issue was circumvented by superimposing thymine on the aromatic, six-membered ring of Fapy·dG to compute the endocyclic overlap areas. It is noteworthy that no such problem occurred for computation of the overlap areas involving all-atoms, or for any other base, including 8-oxo-dG.

MD trajectories with DNA in pol β were conducted with the Verlet algorithm in CHARMM, using a 10 Å cutoff applied to the non-bonded Lennard-Jones interactions. The SHAKE algorithm (36) was used to constrain bonds with hydrogen atoms using a tolerance of 0.0005 Å. A time step of 2 fs was used in the dynamics simulations. A full −1.0 charge was included on phosphates.

The X-ray structure of pol β with *anti*-8-oxo-G paired with dCTP [1MQ3 in the RCSB Protein Data Bank (37)] was converted to a CHARMM 27 file. This structure has three strands of DNA, which can be thought of as a template strand with a one base gap in the primer strand, where the gap is occupied by the dNTP in the active site. The bases in the X-ray structure were changed to give the 5-T**G**T sequence context (5′-GCAGTXTCAGCTCAGC/5′-GCTGAGCTGA[gap with dNTP]ACTGC, where 'X' is 8-oxo-G or Fapy·G). To the 73 water molecules in the X-ray structure, two layers of TIP3P water were added (using the Soak utility in Insight II) around the DNA not in contact with protein, as the surface of this DNA is recessed in comparison with the surface of the

protein. Finally, three more layers of water were added around the protein and the hydrated DNA, which gave a smooth, coherent solvent shell with 2133 total waters. Ions present in the pol β structure were retained, but no counter ions were added, which we call as the 'unrefined input X-ray structure'. Water alone was minimized [2000 steps of ABNR (adopted basis Newton–Raphson)] to allow it to settle into the protein, and then the entire ensemble was minimized (200 steps of ABNR) to allow the bases in the new DNA sequence to adapt to the rest of the structure. The structure was heated to 300 K over 20 ps using the Verlet algorithm, and MD was conducted at 300 K on the protein alone for 50 ps to allow the protein to adapt to the unnatural DNA bases, notably 8-oxo-dG and Fapy·dG in the *syn*-conformation, which protrude into the minor groove far enough to have a slight van der Waals contact with R283, and the latter adapts by moving almost imperceptibly. Thereafter, MD was continued without constraints for 100 ps. The structure reached equilibrium relatively quickly (<50 ps, Supplementary Figure S1), which we attribute to the fact that the initial input structure came from X-ray coordinates. Subsequently, the structure was minimized (200 steps of ABNR) to remove distortions due to the elevated temperatures and to generate the final structures, which were evaluated. The unrefined input X-ray structure in the 5′-TGT sequence with template *anti*-8-oxo-G was converted to *syn*-8-oxo-G (i.e. O4′-C1′-N9-C4 was changed from −111.5 to 70.1) and dCTP was converted to dATP, after which the protocol was repeated. The 8-oxo-G residue was also replaced in the unrefined input X-ray structure with Fapy·G, and the identical protocol was followed for both *anti*-Fapy·G:dCTP (O4′-C1′-N9-C4 = −94.1) and *syn*-Fapy·G:dATP (O4′-C1′-N9-C4 = 102.1). *syn*-Fapy·G:dATP is most distantly related to the original X-ray structure (i.e. *anti*-8-oxo-G:dCTP), so we extended this MD trajectory to 180 ps; however, the structure remained at equilibrium (Supplementary Figure S1).

Each final structure (i.e. *anti*-8-oxo-G:dCTP, *syn*-8-oxo-G:dATP, a*nti*-Fapy·G:dCTP and *syn*-Fapy·G:dATP) in the 5′-TGT sequence was converted to the 5′-TGA sequence using the free energy perturbation (FEP) protocol that we developed recently (38).

For the 8-oxo-dA structure, *syn*-8-oxo-dG and its complementary dATP were converted to *syn*-8-oxo-dA and dGTP, respectively, by using the atom replacement function in Insight II. An MD trajectory had not been performed. Our goal in this part of the work was to determine if a reasonable hydrogen bonded structure would be possible with *syn*-8-oxo-A:dGTP (in contrast to *syn*-8-oxo-dG:dATP), and to test the hypothesis that a structural perturbation must occur before a dGTP could be satisfactorily opposite *syn*-8-oxo-dA.

RESULTS

Construction and characterization of single-stranded pMS2 vector containing Fapy·dG, 8-oxo-dG, or dG as well as Fapy·dA, 8-oxo-dA or dA

Biological effects of many DNA damages have been studied by using the pMS2 vector [(39–41) and references therein] and the strategy for employing this plasmid is shown in Scheme 2. Briefly, the pMS2 ssDNA was digested with EcoRV and the linear DNA was hybridized with a 58mer scaffold to yield a gapped DNA. The dodecamers containing unmodified (dG or dA) or modified (Fapy·dG, 8-oxo-dG, Fapy·dA or 8-oxo-dA) nucleosides were ligated to this gap. The control and lesion containing constructs were treated with exonuclease III and T4 DNA polymerase to remove the scaffold. A portion of each of these vectors was run on a 1% agarose gel. As shown in Figure 1, lanes 1 and 2 show migration characteristics of pMS2 DNA before and after digestion with EcoRV. Lanes 3–5 show ligation of control, 8-oxo-dG and Fapy·dG

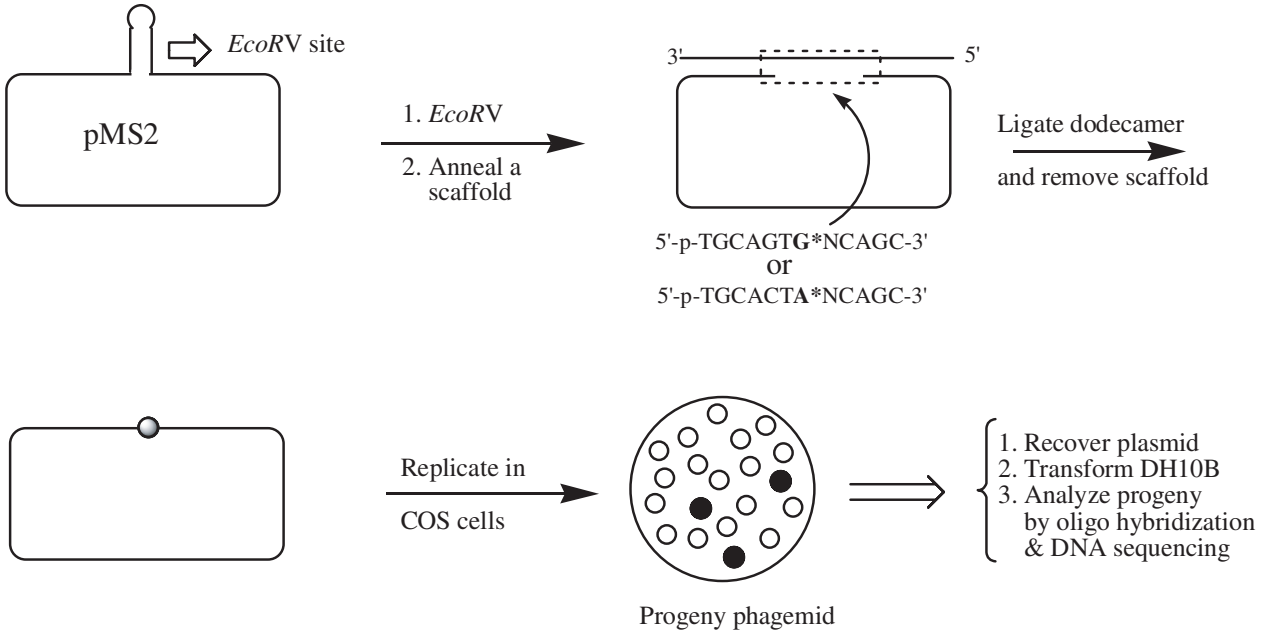

Scheme 2. A general scheme of construction, replication and analysis of the control and modified single-stranded pMS2 vectors.

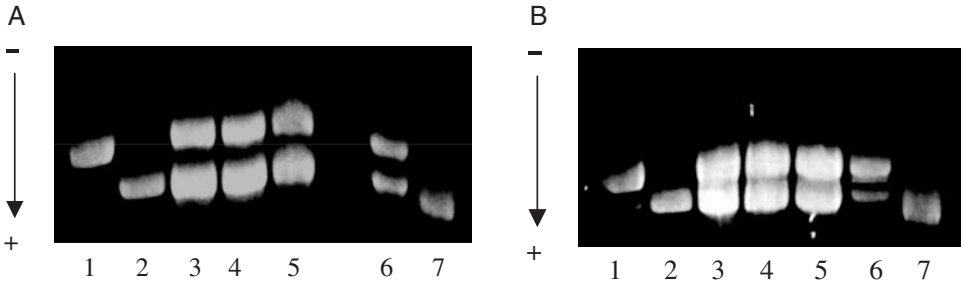

Figure 1. (**A** and **B**) show the constructs with 5′-TGT and 5′-TGA sequence, respectively. Lanes 1 and 2, pMS2 DNA before and after digestion with EcoRV. Lanes 3–5 show pMS2 constructs containing dG, 8-oxo-dG and Fapy·dG, respectively, after enzymatic removal of the scaffold 58mer. Lanes 6 and 7 represent, before and after the removal of the scaffold, respectively, of a 'mock' ligation mixture, which did not contain a dodecamer.

Table 1. Comparative mutagenesis of Fapy·dG and 8-oxo-dG in simian kidney cells

Experiment	Insert	No. of colonies screened	G→T mutation (%)	G→C mutation (%)
1	TGA	117	0 (0)	0 (0)
1	T(Fapy·G)A	284	23 (8.1)	0 (0)
2	T(Fapy·G)A	201	17 (8.5)	0 (0)
Total	T(Fapy·G)A	485	40 (8.2)	0 (0)
1	T (8-oxo-G)A	152	10 (6.6)	0 (0)
2	T (8-oxo-G)A	159	9 (5.7)	0 (0)
Total	T (8-oxo-G)A	311	19 (6.1)	0 (0)
1	TGT	97	0 (0)	0 (0)
2	TGT	142	0 (0)	0 (0)
Total	TGT	239	0 (0)	0 (0)
1	T(Fapy·G)T	177	45 (25.4)	4 (2.3)
2	T(Fapy·G)T	181	61 (33.7)	0 (0)
Total	T(Fapy·G)T	358	106 (29.6)	4 (1.1)
1	T (8-oxo-G)T[a]	326	78 (23.9)	0 (0)
2	T (8-oxo-G)T[a]	271	62 (22.9)	1 (0.4)
Total	T (8-oxo-G)T[a]	597	140 (23.5)	1 (0.2)

[a]Data taken from Ref. (42).

Table 2. Comparative mutagenesis of Fapy·dA and 8-oxo-dA in simian kidney cells

Experiment	Insert	No. of colonies screened	A→A* [No mutation] (%)	A*→C mutation (%)
1	TAA	208	208 (100)	0 (0)
2	TAA	78	78 (100)	0 (0)
Total	TAA	286	286 (100)	0 (0)
1	T(Fapy·A)A	161	161 (100)	0 (0)
2	T(Fapy·A)A	120	119 (99.2)	1 (0.8)
Total	T(Fapy·A)A	281	280 (99.6)	1 (0.4)
1	T(8-oxo-A)A	143	141 (98.6)	2 (1.4)
2	T(8-oxo-A)A	120	120 (100)	0 (0)
Total	T(8-oxo-A)A	263	261 (99.2)	2 (0.8)
1	TAT	97	97	0 (0)
2	TAT	99	99	0 (0)
Total	TAT	196	196	0 (0)
1	T(Fapy·A)T	118	118	0 (0)
2	T(Fapy·A)T	100	100	0 (0)
Total	T(Fapy·A)T	218	218	0 (0)
1	T(8-oxo-A)T	95	95	0 (0)
2	T(8-oxo-A)T	127	127	0 (0)
Total	T(8-oxo-A)T	222	222	0 (0)

containing dodecamers, respectively, to pMS2 followed by enzymatic removal of the scaffold. Lanes 6 and 7 represent, before and after removal of the scaffold, respectively, of a 'mock' ligation mixture, in which no oligonucleotide was added. Estimation of the relative intensity of the circular and linear DNA indicated ∼45% ligation of the 12mers occurred on both sides and that ligation efficiencies of the control and lesion containing oligonucleotides were approximately the same. The results with the Fapy·dA, 8-oxo-dA and dA oligonucleotides were similar (data not shown).

Mutagenicity of Fapy·dG and 8-oxo-dG in simian kidney cells

Following purification, the site-specifically altered pMS2 vectors (50 ng) were transfected in COS-7 cells by electroporation. The progeny plasmids were isolated and used to transform *E.coli* DH10B. The transformants were selected at random and analyzed by oligonucleotide hybridization, followed by DNA sequencing. As shown in Table 1, two independent phagemid constructs showed similar results. Incorporation of the correct nucleotide, dCMP, occurred preferentially (>70%) opposite Fapy·dG, but significant misincorporation was also detected. In the 5′-TGT sequence, Fapy·G→T occurred at 25–30% frequency, and ∼2% Fapy·G→C was detected in one experiment. In the 5′-TGA sequence, in contrast, Fapy·G→T was observed at only about 8% frequency. It is noteworthy that 8-oxo-G→T transversion was also similarly influenced by the sequence context such that 23–24% mutations occurred in 5′-TGT sequence relative to 6% in the 5′-TGA sequence. No mutants were detected from the control constructs.

Mutagenicity of Fapy·dA and 8-oxo-dA in simian kidney cells

In contrast to the results of Fapy·dG and 8-oxo-dG, no mutants were detected from the Fapy·dA and 8-oxo-dA constructs in the 5′-TAT sequence (Table 2). However, in 5′-TAA sequence of the total 263 colonies analyzed, 2 A→C mutants were isolated from the 8-oxo-dA construct [mutational frequency (MF) 0.8%], whereas for the Fapy·dA, of the 281 colonies, only one A→C mutant was found (MF 0.4%). We conclude that both Fapy·dA and 8-oxo-dA are only very weakly mutagenic in certain sequences.

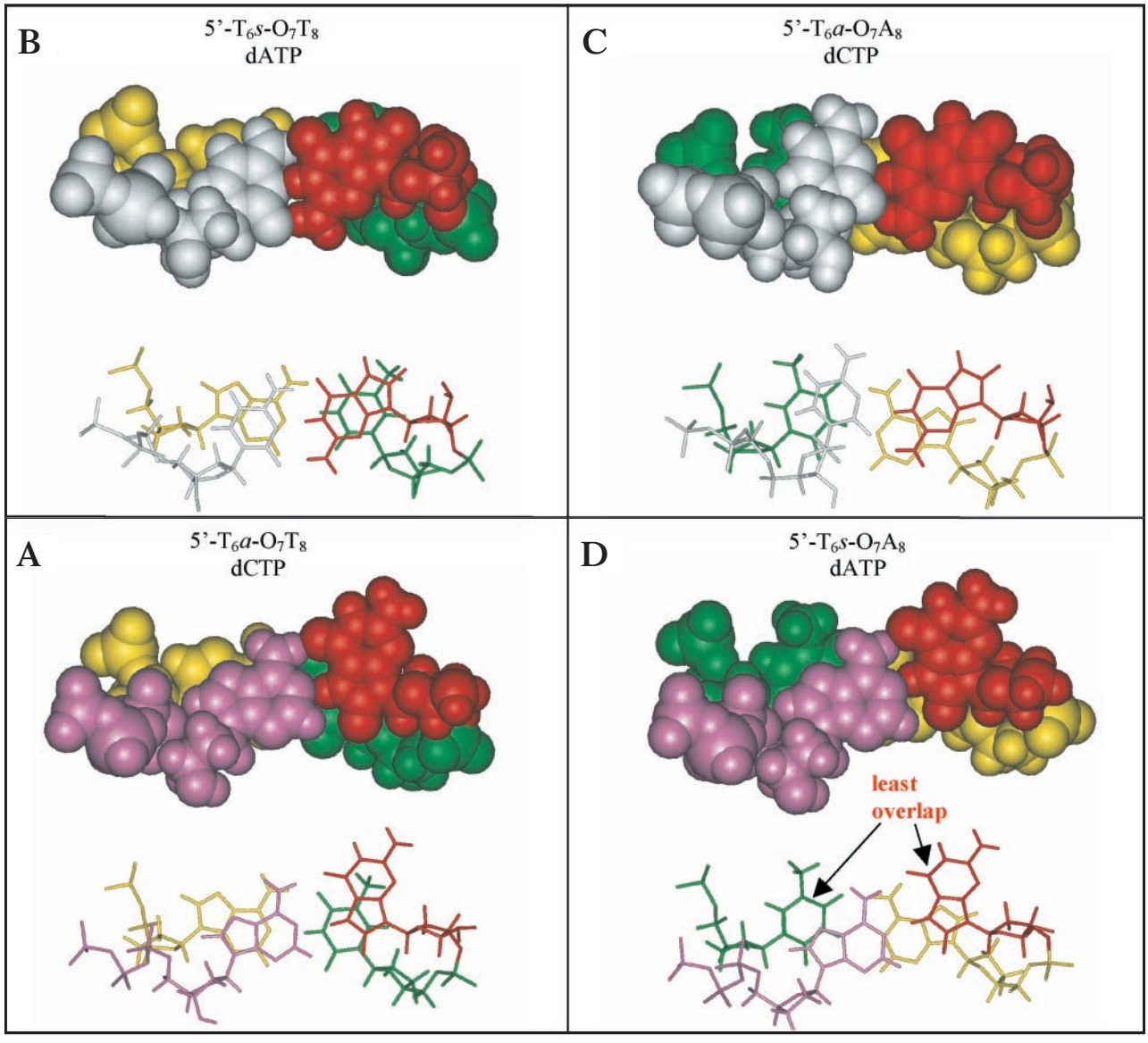

Figure 2. *anti*-8-Oxo-G opposite dCTP (**A** and **C**) and *syn*-8-oxo-G opposite dATP (**B** and **D**) in the 5′-TGT and 5′-TGA sequences in the active site of pol β, following MD. Only the base pairs involving 8-oxo-G and the dNTP are shown, along with the base pair on the 3′-side of the 8-oxo-G. The bases are 8-oxo-G (red), A (yellow) and T (green), dCTP (gray) and dATP (purple).

Molecular modeling of 8-oxo-dG

Several earlier site-specific studies showed that the mutation frequency of 8-oxo-G in ssDNA in simian kidney cells was in the range 4–7%, inducing primarily G→T transversions [reviewed in Ref. (8)]. We were surprised that 8-oxo-G in the 5′-TGT sequence context generates progeny with 23–24% G→T mutations in the 5′-TGT sequence context in COS cells (42). This is several-fold higher than the 5′-TGA sequence studied by us (Table 1) and other sequence contexts studied by Moriya, Grollman and coworkers (23,43). We did molecular modeling in the active site of a DNA polymerase to investigate whether there might be a structural difference that could provide a hypothesis for why G→T mutations for 8-oxo-dG in a 5′-TGT sequence were higher than in a 5′-TGA sequence. Bypass is generally believed to involve non-mutagenic pairing of *anti*-8-oxo-G with dCTP, and mutagenic pairing of *syn*-8-oxo-G with dATP (37,44,45); hence we focused on these structures.

The X-ray structure of DNA polymerase β (pol β) with dCTP opposite *anti*-8-oxo-G was used as a starting point. The X-ray DNA sequence was modified to the appropriate 5′-TGT context and an MD trajectory was conducted in the presence of water (for details see Materials and Methods). Coordinates for a typical low-energy structure from the MD trajectory was compared with the X-ray starting coordinates and r.m.s.d. = 0.98 Å was determined for the protein (DNA was excluded because of the sequence difference), showing that the methodology did not significantly affect the structure. *anti*-8-oxo-G was converted to *syn*-8-oxo-G and dCTP converted to dATP, and an MD trajectory was conducted in pol β in the 5′-TGT sequence. Following the MD runs for both

anti-8-oxo-G:dCTP and *syn*-8-oxo-G:dATP, a FEP approach that we developed recently (38) was used to convert the sequence from 5′-TGT to 5′-TGA, by changing the base pair on the 3′-side from T:A to A:T. FEP is recognized as an effective way of comparing closely related structures, as the atoms to be changed in the starting structure are gradually faded out, while the atoms in the final structure are faded in, which thereby minimizes gratuitous differences in the structures. When the four structures were compared, interesting differences in stacking were noted between the bases in the [*n*] position (i.e. 8-oxo-G and the dNTP) and the [*n* + 1] position (i.e. the base pair on the 3′-side). The *syn*-8-oxo-G:dATP structure had better stacking with the 3′-T:A base pair in the 5′-TGT sequence (Figure 2B) than it did with the 3′-A:T base pair in the 5′-TGA sequence (Figure 2D). The extent of this stacking was quantified by measuring van der Waals surface overlap (7.03 versus 4.13 Å^2, respectively, Table 3). In contrast, van der Waals surface overlap was more similar for *anti*-8-oxo-G:dCTP in the 5′-TGT (Figure 2A) versus 5′-TGA (Figure 2C) sequences (10.50 versus 9.28 Å^2, respectively, Table 3). A similar trend in stacking was also observed when just the atoms contributing to the π-cloud were considered (Table 3). If these stacking differences were expressed during the insertion step, then dATP would be incorporated less efficiently in a 5′-TGA sequence relative to 5′-TGT. This observation provides a rationale for the mutagenesis results, and the hypothesis could be tested in future experiments. [A discussion in Supplementary Data has been included to point out that such stacking is likely to be inherent in the structure of DNA and has not been imposed by pol β (Supplementary Table S2).] It is noteworthy that 3′-templating base stabilizing the active site of pol β through stacking interactions have been suggested to play critical roles in the catalytic efficiency and fidelity of the polymerase in several earlier investigations (46,47).

In duplex DNA, *anti*-G:*anti*-A has been observed in addition to *syn*-G:*anti*-A with the corresponding unmodified bases (48–51), and both pairings have two hydrogen bonds. Without a major disruption in protein structure, it was not possible for the active site of pol β to accommodate the *anti*-purine:*anti*-purine arrangement required to pair *anti*-8-oxo-G with *anti*-A in dATP, and, thus, we did not study this pairing arrangement. In fact, DNA polymerase structure probably evolved to make such purine:purine pairings unfavorable.

Table 3. van der Waals overlap between the base pair containing 8-oxo-G or Fapy·G and the base pair on the 3′-side computed using structures developed by molecular modeling in the active site of pol β[a]

	anti-8-oxo-G:dCTP	*anti*-Fapy·G:dCTP
5′-TGT	10.50 (3.35)	10.66 (3.21)
5′-TGA	9.28 (3.06)	10.99 (4.94)
	syn-8-oxo-G:dATP	*syn*-Fapy·G:dATP
5′-TGT	7.03 (4.27)	11.86 (4.87)
5′-TGA	4.13 (1.45)	5.96 (0.61)

[a]The X-ray structure of *anti*-8-oxo-G:dCTP in the active site of pol β was used as the starting point to construct models for each of the indicated base pairs in the 5′-TGT sequence context used in the mutagenesis study (Materials and Methods). Thereafter, a MD run was conducted with water and counter ions. The lowest energy structure from the MD run was used to compute the van der Waals overlap area (Materials and Methods) between the 8-oxo-G:dCTP base pair and T:A base pair on the 3′-side; the value reported in the table is in units of Angstroms squared. The van der Waals overlap areas were computed for all-atoms and endocyclic (aromatic) atoms (parentheses) in each base using 3DNA.

Molecular modeling of Fapy·dG

A parallel molecular modeling study with Fapy·G in duplex DNA was conducted. The van der Waals surface overlap between adjacent base pairs in the active site of pol β with *anti*-Fapy-G:dCTP and *syn*-Fapy·G:dATP was also compared in a manner analogous to our study with 8-oxo-G. After MD, *syn*-Fapy·G:dATP showed more efficient stacking in the 5′-TGT versus 5′-TGA sequence (11.86 versus 5.96 Å^2, Table 3), while the stacking for *anti*-Fapy·G:dCTP was similar in these two sequence contexts (10.66 versus 10.99 Å^2, Table 3). This difference is apparent in Figure 3, which shows the stacking between the relevant adjacent base pairs for the four Fapy·dG structures (i.e. with dCTP and dATP in the 5′-TGT and 5′-TGT sequences). This observation provides a rationale for why dATP incorporation in the 5′-TGA sequence might be disfavored, which is consistent with the mutagenesis results (Table 1). The validity of this structural explanation can be evaluated in future experiments.

Molecular modeling of 8-oxo-dA

MF of 8-oxo-dA was significantly lower than 8-oxo-dG, and the only type of mutation detected with 8-oxo-dA was the A→C transversion (Table 2). To investigate a possible rationale for this lower MF, *syn*-8-oxo-dG was converted (without MD) to *syn*-8-oxo-dA, and dATP to dGTP in the active site of pol β (Figure 4). Hydrogen bonding was not observed, and there was a steric crowding between HN7 of *syn*-8-oxo-dA (red) with HN1 of dGTP (purple). There are two ways that this crowding could be minimized. One way is to deprotonate one of the nitrogens. However, this necessitates an energy penalty, resulting in a higher energy structure and a correspondingly lower MF would be expected. A second possibility is that the *syn*-8-oxo-A:dGTP pair could form a wobble base pair. Because of the positioning of R283 (dark blue) and Y271 (blue), the dGTP cannot move, which implies that *syn*-8-oxo-dA would have to move toward the major groove (upward in Figure 4), where there may be room before encountering I33 (green) and H34 (dark green). A wobble structure is inherently higher in energy than a Watson–Crick pair, which would result in a less frequent dGTP insertion and a lower MF.

DISCUSSION

The current study showed that Fapy·dG was strongly mutagenic in simian kidney cells, whereas Fapy·dA was very weakly mutagenic. Earlier reports on the mutagenicity of 8-oxo-dG relative to 8-oxo-dA showed a similar trend in that the former is approximately an order of magnitude more mutagenic than the latter (43,52), which we also noted in the current study. Fapy·dG primarily induced G→T transversions, and it was 25–35% more mutagenic than 8-oxo-dG. However, both lesions showed a similar sequence context effect in that nearly a 4-fold greater number of mutations occurred in the 5′-TGT sequence relative to 5′-TGA. Mutagenicity of 8-oxo-dG determined in a number of studies in *E.coli* and in mammalian cells showed that it predominantly induces G→T transversions

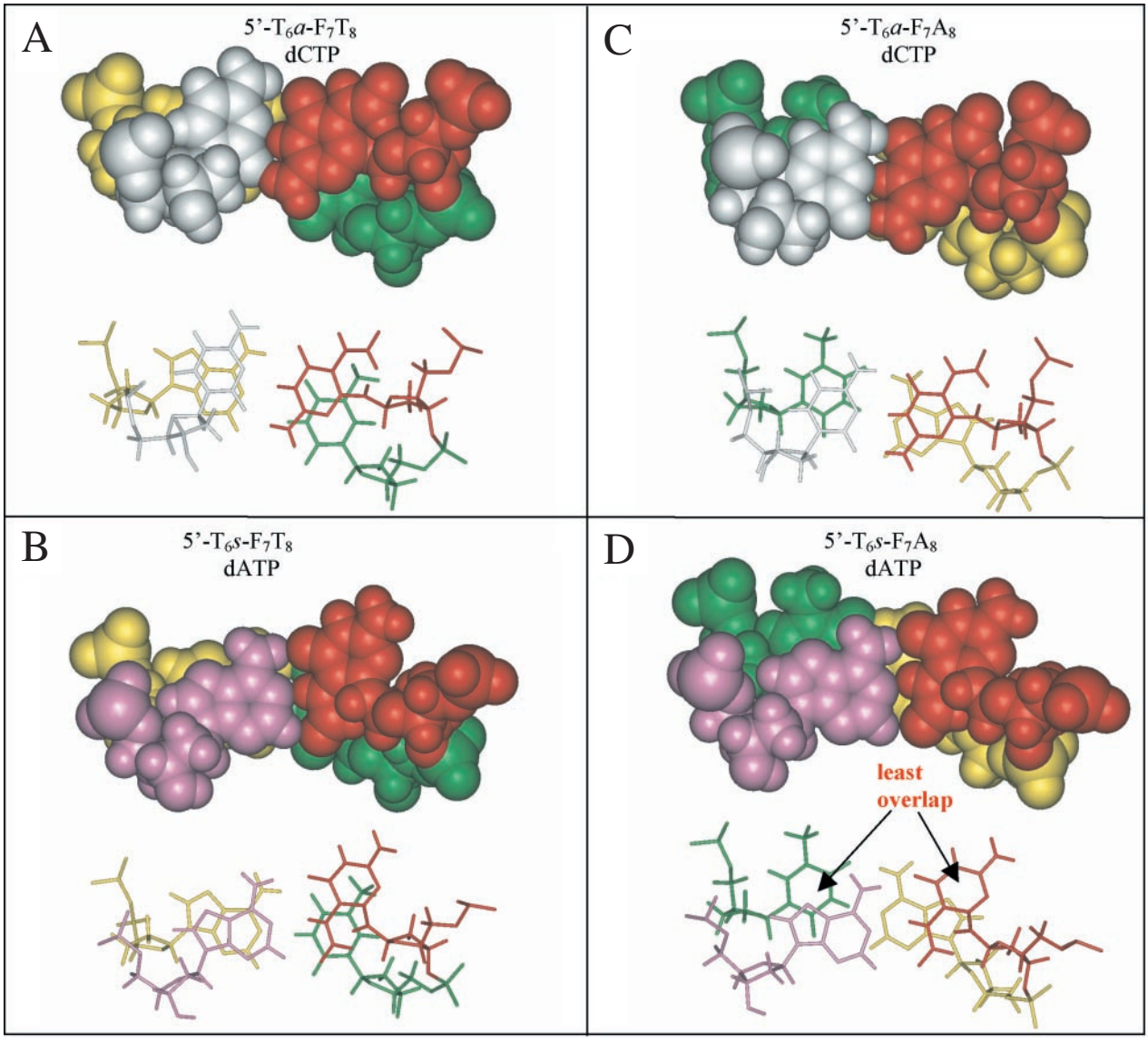

Figure 3. *anti*-Fapy-G opposite dCTP (**A** and **C**) and *syn*-Fapy-G opposite dATP (**B** and **D**) in the 5′-TGT and 5′-TGA sequences in the active site pol β, following MD. Only the base pairs involving Fapy·G and the dNTP are shown, along with the base pair on the 3′-side of the Fapy-G. The bases are Fapy·G (red), A (yellow) and T (green), dCTP (gray) and dATP (purple).

(23,43,52–55). The MF of 8-oxo-dG as determined in the site-specific studies falls in the range of 3–8% in ssDNA in both bacterial and mammalian cells (23,43,52–55). In double-stranded DNA the MF is much lower (56), presumably due to more efficient repair. However, the combined effects of differential repair and variable miscoding efficiency in different sequences may result in up to 10^2- to 10^3-fold differences in the mutagenic potential of 8-oxo-dG (57). While the MF of 8-oxo-dG in the 5′-TGA sequence was similar to what others found in COS cells, we serendipitously discovered that the MF is nearly 4-fold higher in the 5′-TGT sequence (42). Could this increase in MF for both Fapy·dG and 8-oxo-dG be due to inefficient repair in the 5′-TGT sequence? Although this study was done in ssDNA, COS cells have a functional analog of MutY protein, which removes adenines from 8-oxo-G:A pairs after DNA replication is completed. We cannot rule out that compared with a 3′-A:T base pair, a 3′-T:A base pair would result in significantly slower repair of Fapy·G:A and 8-oxo-G:A mispairs. Even so, elevated miscoding of 8-oxo-dG in certain sequences has been demonstrated (57), and we consider this a more likely scenario.

Since structural or modeling studies of the other sequences studied earlier have not been reported, we found an opportunity to investigate the subtle differences between an adenine and a thymine 3′ to the 8-oxo-G of an otherwise identical sequence. Our modeling results provided a possible rationale for why G→T mutations were lower in the 5′-TGA sequence; 8-oxoG:A and Fapy-G:A base pair stacked relatively poorly with the base pair on the 3′-side in a 5′-TGA sequence compared with a 5′-TGT sequence (Figures 2 and 3 and Table 3). This structural hypothesis can be tested in future studies. We chose to model 8-oxo-G and Fapy·G in pol β because, when we

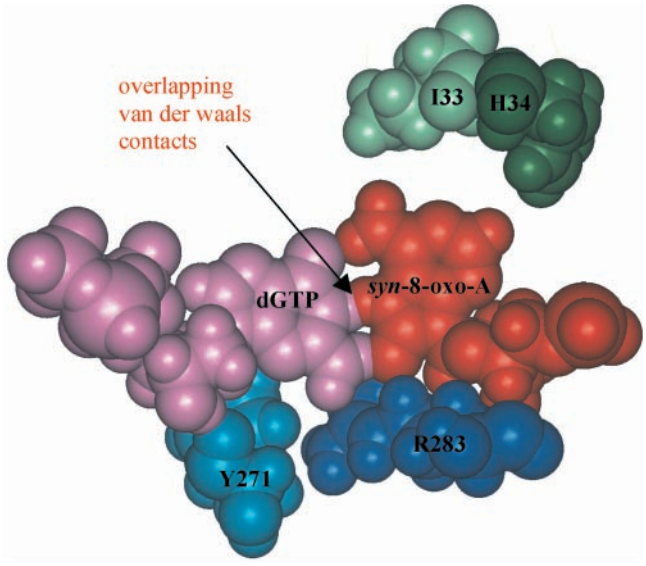

Figure 4. *syn*-8-Oxo-A (red) opposite dGTP (purple) in the active site pol β. Following MD, a *syn*-8-oxo-G:dATP structure (5′-T**G**T sequence) was converted to *syn*-8-oxo-A:dGTP by simple base replacement. In the base pairing region, overlapping van der Waals contacts are apparent. A wobble is one way to generate a reasonable hydrogen bonded structure (see text). The dGTP (purple) cannot wobble toward the minor groove because of R283 (blue) and Y271 (light blue), so *syn*-8-oxo-A (red) would have to wobble toward the major groove, in which there is enough room because of the positioning of I33 (green) and H34 (dark green).

initiated our molecular modeling study it was the only DNA polymerase with an X-ray structure containing a template 8-oxo-G to use as a starting structure (37). The choice is also reasonable given that pol β bypasses 8-oxo-G and inserts both dCTP and dATP (44). The disadvantage is that either a replicative B-family polymerase or a lesion-bypass Y-family polymerase is more likely to be involved in 8-oxo-G bypass in COS cells, although this has not been unequivocally established. No X-ray structure was available for a replicative eukaryotic B-family polymerase, although an X-ray structure for RB69, the B-family polymerase from bacteriophage T4, with 8-oxo-G containing DNA has been reported (58). Since the initiation of our molecular modeling study, an X-ray structure containing dCTP opposite template 8-oxo-G was published for T7 DNA polymerase (45), an A-family DNA polymerase. Subsequently, crystal structures of the complexes with the Y-family polymerase Dpo4, which predominantly incorporates dCTP opposite 8-oxo-dG, have also been reported (59,60). Examination of some of these structures (Supplementary Figure S4) revealed no obvious reason why the results with 8-oxo-G:dNTP base pairs with pol β (of the X-family) would be qualitatively different than with a polymerase in the B-family, Y-family, or A-family, although additional studies are required to address this point.

It is important to consider the caveats in our modeling results. Fapy·dG may adopt a variety of rotational isomers, and we have only explored a subset of them by modeling, although we did study both eclipsing versions of the two rotational isomers that are favored in solution (34). Furthermore, we have not explored more extensive MD trajectories in our modeling. We cannot rule out that lower energy conformations might be discovered that negate the correlation between the higher fraction of G→T mutations in 5′-TGT sequences and the increased stacking overlap between 8-oxo-G:A (or Fapy·G:A) and the base pair on the 3′-side in the 5′-TGT sequence. While this is admittedly a formal possibility, an inspection of our models (Figures 2 and 3) suggests that the backbone coordinates of the 8-oxo-G:A and Fapy·G:A structures would have to change dramatically to allow comparable overlaps in 5′-TGA versus 5′-TGT sequences, making this possibility unlikely. The relatively nonmutagenic nature of the 8-oxo-dA was also consistent with the model at the active site of pol β (Figure 4). Given the outcome of our modeling, one logical next step would be to establish which DNA polymerase is involved in the insertion step opposite 8-oxo-dG (and Fapy·dG) in COS cells, after which we could probe more deeply whether our hypothesis about the mechanism is correct. Regrettably, as yet we do not know which DNA polymerase bypasses 8-oxo-G (and Fapy·dG) in a cell. Despite the discovery of several bypass polymerases in the last few years [reviewed recently in Ref. (61)], our understanding of the mechanism of this process, especially in eukaryotic cells, remains fragmentary and incomplete. More recently, the question of whether more than one polymerase can be involved in the translesion synthesis has become a hot topic of discussion (62). Therefore, determination of the mechanistic details of mutagenesis by these lesions must await further advances in this area of research.

For Fapy·dG, NMR and crystallographic investigations have yet to be carried out. However, a DNA melting study using the same set of 12mers that have been used in this investigation showed that dC opposite this lesion is most stable followed by dA > dG > dT (20). *In vitro* primer extension study using Klenow fragment also showed that dCMP is the most preferred nucleotide, but discrimination against dAMP incorporation is not high (20). The preference of nucleotide incorporation noted in the current study followed the same trend in that dCMP was incorporated >70% followed by dAMP (8 or 30% depending on the sequence). Even though elucidating the mutagenic mechanism of Fapy·dG requires further structural and biochemical studies, our finding that it is a potent mutagenic lesion in mammalian cells relative to the three other oxidative damages studied in this work underscores its biological importance.

In conclusion, this study demonstrates for the first time that in identical sequence contexts Fapy·dG induces G→T substitutions at a higher frequency than 8-oxo-dG in a mammalian cell. In contrast, Fapy·dA is very weakly mutagenic, much like 8-oxo-dA is, and both lesions induce A→C in a 5′-T*A*A sequence context. Modeling studies suggest the importance of base stacking in nucleotide misincorporations, which appears to depend on the local DNA sequence. Additional studies will be required to validate this hypothesis.

SUPPLEMENTARY DATA

Supplementary Data are available at NAR Online.

ACKNOWLEDGEMENTS

This study was supported by NIEHS grants ES09127 and ES013324 (to A.K.B), ES03775 (to E.L.L.) and NCI grants

CA74954 (to M.M.G), CA50432 (to E.L.L.), and CA76163 and CA47995 (to M.M.). Funding to pay the Open Access publication charges for this article was provided by NIEHS (grant ES013324).

Conflict of interest statement. None declared.

REFERENCES

1. Beckman,K.B. and Ames,B.N. (1997) Oxidative decay of DNA. *J. Biol. Chem.*, **272**, 19633–19636.
2. Anson,R.M., Sentürker,S., Dizdaroglu,M. and Bohr,V.A. (1999) Measurement of oxidatively induced base lesions in liver nuclear and mitochodrial DNA from Wistar rats of different ages. *Free Radic. Biol. Med.*, **27**, 456–462.
3. Cooke,M.S., Evans,M.D., Dizdaroglu,M. and Lunec,J. (2003) Oxidative DNA damage: mechanisms, mutation, and disease. *FASEB J.*, **17**, 1195–1214.
4. Téoule,R. (1987) Radiation induced DNA damage and its repair. *Int. J. Radiat. Biol.*, **51**, 573–589.
5. Breen,A.P. and Murphy,J.A. (1995) Reactions of oxyl radical with DNA. *Free Radic. Biol. Med.*, **18**, 1033–1077.
6. Cadet,J., Berger,M., Douki,T. and Revanat,J.-L. (1997) Oxidative damage to DNA: formation, measurement and biological significance. *Rev. Physiol. Biochem. Pharmacol.*, **31**, 1–87.
7. Dizdaroglu,M. (1992) Oxidative damage to DNA in mammalian chromatin. *Mutat. Res.*, **275**, 331–342.
8. Kamiya,H. (2003) Mutagenic potentials of damaged nucleic acids produced by reactive oxygen/nitrogen species: Approaches using synthetic oligonucleotides and nucleotides. *Nucleic Acids Res.*, **31**, 517–531.
9. Steenken,S. (1989) Purine bases, nucleosides, and nucleotides: aqueous solution redox chemistry and transformation reactions of their radical cations and e- and OH adduct. *Chem. Rev.*, **89**, 503–520.
10. Candeias,L.P. and Steenken,S. (2000) Reaction of HO. with guanine derivatives in aqueous solution: formation of two different redox-active OH-adduct radicals and their unimolecular transformation reactions. Properties of G(-H). *Chem. Eur. J.*, **6**, 475–484.
11. Pouget,J.-P., Douki,T., Richard,M.-J. and Cadet,J. (2000) DNA damage induced in cells by and UVA radiation as measured by HPLC/GC-MS and HPLC-EC and comet assay. *Chem. Res. Toxicol.*, **13**, 541–549.
12. Dizdaroglu,M., Jaruga,P., Birincioglu,M. and Rodriguez,H. (2002) Free-radical-induced damage to DNA: mechanisms and measurements. *Free Radic. Biol. Med.*, **32**, 1102–1115.
13. Boiteux,S., Gajewski,E., Laval,J. and Dizdaroglu,M. (1992) Substrate specificity of the *Escherichia coli* Fpg protein formamidopyrimidine-DNA glycosylase: excision of purine lesions in DNA produced by ionizing radiation or photosensitization. *Biochemistry*, **31**, 106–110.
14. Gajewski,E., Rao,G., Nackerdien,Z. and Dizdaroglu,M. (1990) Modification of DNA bases in mammalian chromatin by radiation-generated free radicals. *Biochemistry*, **29**, 7876–7882.
15. Raoul,S., Bardet,M. and Cadet,J. (1995) γ Irradiation of 2′-deoxyadenosine in oxygen-free aqueous solutions: Identification and conformational features of formamidopyrimidine nucleoside derivatives. *Chem. Res. Toxicol.*, **8**, 924–933.
16. Cadet,J., Bellon,S., Douki,T., Frelon,S., Gasparutto,D., Muller,E., Pouget,J.-P., Ravanat,J.-L., Romieu,A. and Sauvaigo,S. (2004) Radiation-induced DNA damage: formation, measurement, and biochemical features. *J. Environ. Pathol. Toxicol. Oncol.*, **23**, 33–43.
17. Haraguchi,K. and Greenberg,M.M. (2001) Synthesis of oligonucleotides containing Fapy·dG (*N6*-(2-deoxy-α,β-D-*erythro*-pentofuranosyl)-2,6-diamino-4-hydroxy-5-formamidopyrimidine). *J. Am. Chem. Soc.*, **123**, 8636–8637.
18. Jiang,Y.L., Wiederholt,C.J., Patro,J.N., Haraguchi,K. and Greenberg,M.M. (2005) Synthesis of oligonucleotides containing Fapy·dG (N^6-(2-deoxy-α, β-D-erythropentofuranosyl)-2,6-diamino-4-hydroxy-5-formamidopyrimidine) using a 5′-dimethoxytrityl dinucleotide phosphoramidite. *J. Org. Chem.*, **70**, 141–149.
19. Haraguchi,K., Delaney,M.O., Wiederholt,C.J., Sambandam,A., Hantosi,Z. and Greenberg,M.M. (2002) Synthesis and characterization of oligodeoxynucleotides containing formamidopyrimidine lesions and nonhydrolyzable analogues. *J. Am. Chem. Soc.*, **124**, 3263–3269.
20. Wiederholt,C.J. and Greenberg,M.M. (2002) Fapy·dG instructs Klenow exo$^-$ to misincorporate deoxyadenosine. Fapy·dG instructs Klenow exo- to misincorporate deoxyadenosine. *J. Am. Chem. Soc.*, **124**, 7278–7279.
21. Delaney,M.O., Wiederholt,C.J. and Greenberg,M.M. (2002) Fapy·dA induces nucleotide misincorporation translesionally by a DNA polymerase. *Angew. Chem. Int. Ed.*, **41**, 771–773.
22. Wiederholt,C.J., Delaney,M.O., Pope,M.A., David,S.S. and Greenberg,M.M. (2003) Repair of DNA containing Fapy·dG and its β-C-nucleoside analogue by formamidopyrimidine DNA glycosylase and mutY. *Biochemistry*, **42**, 9755–9760.
23. Moriya,M. (1993) Single-stranded shuttle phagemid for mutagenesis studies in mammalian cells: 8-oxoguanine in DNA induces targeted G.C→T.A transversions in simian kidney cells. *Proc. Natl Acad. Sci. USA*, **90**, 1122–1126.
24. Pandya,G. and Moriya,M. (1996) 1, N^6-Ethenodeoxyadenosine, a DNA adduct highly mutagenic in mammalian cells. *Biochemistry*, **35**, 11487–11492.
25. Hirt,B. (1967) Selective extraction of polyoma DNA from infected mouse cell cultures. *J. Mol. Biol.*, **26**, 365–369.
26. Ramos,L.A., Lipman,R., Tomasz,M. and Basu,A.K. (1998) The major mitomycin C-DNA monoadduct is cytotoxic but not mutagenic in *Escherichia coli*. *Chem. Res. Toxicol.*, **11**, 64–69.
27. Insight II, version 98.0 (1998) *Molecular Simulation Inc.,* San Diego.
28. Nilsson,L. and Karplus,M. (1986) Empirical energy functions for energy minimization and dynamics of nucleic acids. *J. Comp. Chem.*, **7**, 591–616.
29. MacKerell,A.D.,Jr, Banavali,N. and Foloppe,N. (2000–2001) Development and current status of the CHARMM force field for nucleic acids. *Biopolymers*, **56**, 257–265.
30. Lee,C.H. and Loechler,E.L. (2003) Molecular modeling of the major benzo[a]pyrene N2-dG adduct in cases where mutagenesis results are known in double stranded DNA. *Mutat. Res.*, **529**, 59–76.
31. Arnott,S., Campbell Smith,P.J. and Chandraselaran,R. (1975) Atomic coordinates and molecular conformations for DNA–DNA, RNA–RNA, and DNA–RNA helices. In Fasman,G.D. (ed.), *Handbook of Biochemistry and Molecular Biology, Vol. II: Nucleic Acids. 3rd edn.* CRC Press, Cleveland, OH, pp. 411–422.
32. Kouchakdjian,M., Bodepudi,V., Shibutani,S., Eisenberg,M., Johnson,F., Grollman,A.P. and Patel,D.J. (1991) NMR structural studies of the ionizing radiation adduct 7-hydro-8-oxodeoxyguanosine (8-oxo-7H-dG) opposite deoxyadenosine in a DNA duplex. 8-Oxo-7H-dG(syn).dA(anti) alignment at lesion site. *Biochemistry*, **30**, 1403–1412.
33. McAuley-Hecht,K.E., Leonard,G.A., Gibson,N.J., Thomson,J.B., Watson,W.P., Hunter,W.N. and Brown,T. (1994) Crystal structure of a DNA duplex containing 8-hydroxydeoxyguanine-adenine base pairs. *Biochemistry*, **33**, 10266–10270.
34. Burgdorf,L.T. and Carell,T. (2002) Synthesis, stability, and conformation of the formamidopyrimidine G DNA lesion. *Chem. Eur. J.*, **8**, 293–301.
35. Lu,X.J. and Olson,W.K. (2003) 3DNA: a software package for the analysis, rebuilding and visualization of three-dimensional nucleic acid structures. *Nucleic Acids Res.*, **31**, 5108–5121.
36. Ryckaert,J.P., Ciccotti,G. and Berendsen,H.J.C. (1977) Numerical integration of Cartesian equations of motion of a system with constraints: molecular dynamics of *n*-alkanes. *J. Comput. Phys.*, **23**, 327–341.
37. Krahn,J.M., Beard,W.A., Miller,H., Grollman,A.P. and Wilson,S.H. (2003) Structure of DNA polymerase β with the mutagenic DNA lesion 8-oxodeoxyguanine reveals structural insights into its coding potential. *Structure (Camb.)*, **11**, 121–127.
38. Chandani,S., Lee,C.H. and Loechler,E.L. (2005) Free energy perturbation methods to study structure and energetics of DNA adducts: results for the major N^2-dG adduct of benzo[a]pyrene in two conformations and different sequence contexts. *Chem. Res. Toxicol.*, **18**, 1108–1123.
39. Moriya,M.., Zhang,W., Johnson,F. and Grollman,A.P. (1994) Mutagenic potency of exocyclic DNA adducts: marked differences between *Escherichia coli* and simian kidney cells. *Proc. Natl Acad. Sci. USA*, **91**, 11899–11903.
40. Fernandes,A., Liu,T., Amin,S., Geacintov,N.E., Grollman,A.P. and Moriya,M. (1998) Mutagenic potential of stereoisomeric bay region (+)-

and (−)-*cis-anti*-benzo[a]pyrene diol epoxide-N^2-2′-deoxyguanosine adducts in *Escherichia coli* and simian kidney cells. *Biochemistry*, **37**, 10164–10172.
41. Sanchez,A.M., Minko,I.G., Kurtz,A.J., Kanuri,M., Moriya,M. and Lloyd,R.S. (2003) Comparative evaluation of the bioreactivity and mutagenic spectra of acrolein-derived α-HOPdG and γ-HOPdG regioisomeric deoxyguanosine adducts. *Chem. Res. Toxicol.*, **16**, 1019–1028.
42. Kalam,M.A. and Basu,A.K. (2005) Mutagenesis of 8-oxoguanine adjacent to an abasic site in simian kidney cells: tandem mutations and enhancement of G→T transversions. *Chem. Res. Toxicol.*, **18**, 1187–1192.
43. Tan,X., Grollman,A.P. and Shibutani,S. (1999) Comparison of the mutagenic properties of 8-oxo-7,8-dihydro-2′deoxyadenosine and 8-oxo-7,8-dihydro-2′-deoxyguanosine DNA lesions in mammalian cells. *Carcinogenesis*, **20**, 2287–2292.
44. Efrati,E., Tocco,G., Eritja,R., Wilson,S.H. and Goodman,M.F. (2003) 'Action-at-a-distance' mutagenesis: 8-oxo-7,8-dihydro-2′-deoxyguanosine causes base substitution errors at neighboring template sites when copied by DNA polymerase β. *J. Biol. Chem.*, **274**, 15920–15926.
45. Brieba,L.G., Eichman,B.F., Kokoska,R.J., Doublie,S., Kunkel,T.A. and Ellenberger,T. (2004) Structural basis for the dual coding potential of 8-oxoguanosine by a high-fidelity DNA polymerase. *EMBO J.*, **23**, 3452–3461.
46. Vaisman,A., Warren,M.W. and Chaney,S.G. (2001) The effect of DNA structure on the catalytic efficiency fidelity of human DNA polymerase β on templates with platinum-DNA adducts. *J. Biol. Chem.*, **276**, 18999–19005.
47. Beard,W.A., Shock,D.D., Yang,X.-P., DeLauder,S.F. and Wilson,S.H. (2002) Loss of DNA polymerase β stacking interactions with templating purines, but not pyrimidines, alters catalytic efficiency and fidelity. *J. Biol. Chem.*, **277**, 8235–8242.
48. Kan,L.S., Chandrasegaran,S., Pulford,S.M. and Miller,P.S. (1983) Detection of a guanine X adenine base pair in a decadeoxyribonucleotide by proton magnetic resonance spectroscopy. *Proc. Natl Acad. Sci. USA*, **80**, 4263–4265.
49. Patel,D.J., Kozlowski,S.A., Ikuta,S. and Itakura,K. (1984) Deoxyguanosine–deoxyadenosine pairing in the d(C-G-A-G-A-A-T-T-C-G-C-G) duplex: conformation and dynamics at and adjacent to the dG·dA mismatch site. *Biochemistry*, **23**, 3207–3217.
50. Kennard,O. (1985) Structural studies of DNA fragments: the G.T wobble base pair in A, B and Z DNA; the G.A base pair in B-DNA. *J. Biomol. Struct. Dyn.*, **3**, 205–226.
51. Brown,T., Leonard,G.A., Booth,E.D. and Chambers,J. (1989) Crystal structure and stability of a DNA duplex containing A(anti).G(syn) base-pairs. *J. Mol. Biol.*, **207**, 455–457.
52. Wood,M.L., Estave,A., Morningstar,M.L., Kuziamko,G. and Essigmann,J.M. (1993) Genetic effects of oxidative DNA damage: comparative mutagenesis of 7,8-dihydro-8-oxoguanine and 7,8-dihydro-8-oxoadenine in *Escherichia coli*. *Nucleic Acids Res.*, **20**, 6023–6032.
53. Moriya,M., Qu,C., Bodepudi,V., Johnson,F., Takeshita,M. and Grollman,A.P. (1991) Site-specific mutagenesis using a gapped duplex vector: a study of *in vivo* translesional synthesis past 8-oxodeoxyguanine. *Mutat. Res.*, **254**, 281–288.
54. Le Page,F., Margot,A., Grollman,A.P., Sarasin,A. and Gentil,A. (1995) Mutagenicity of a unique 8-oxoguanine in human Ha-*ras* sequence in mammalian cells. *Carcinogenesis*, **11**, 2779–2784.
55. Henderson,P.T., Delaney,J.C., Muller,J.G., Neeley,W.L., Tannenbaum,S.R., Burrows,C.J. and Essigmann,J.M. (2003) The hydantoin lesions formed from oxidation of 7,8-dihydro-8-oxoguanine are potent sources of replication errors *in vivo*. *Biochemistry*, **42**, 9257–9262.
56. Kamiya,H., Murata-Kamiya,N., Koizume,S., Inoue,H., Nishimura,S. and Ohtsuka,E. (1995) 8-Hydroxyguanine (7,8-dihydro-8-oxoguanine)in hot spots of the c-Ha-*ras* gene: effects of sequence contexts on mutation spectra. *Carcinogenesis*, **16**, 883–889.
57. Hatahet,Z., Zhou,M., Reha-Krantz,L.J., Morrical,S.W. and Wallace,S.S. (1998) In search of a mutational hotspot. *Proc. Natl Acad. Sci. USA*, **95**, 8556–8561.
58. Freisinger,E., Grollman,A.P., Miller,H. and Kisker,C. (2004) Lesion (in)tolerance reveals insights into DNA replication fidelity. *EMBO J.*, **23**, 1494–1505.
59. Zang,H., Irimia,A., Choi,J.-Y., Angel,K.C., Loukachevitch,L.V., Egli,M. and Guengerich,F.P. (2006) Efficient and high fidelity incorporation of dCTP opposite 7,8-dihydro-8-oxodeoxyguanosine by *Sulfolobus solfataricus* DNA polymerase Dpo4. *J. Biol. Chem.*, **281**, 2358–2372.
60. Rechkoblit,O., Malinina,L., Cheng,Y., Kuryavyi,V., Broyde,S., Geacintov,N.E. and Patel,D.J. (2006) Stepwise translocation of Dpo4 polymerase during error-free bypass of an oxoG lesion. *PLoS Biol.*, **4**, e11.
61. Guengerich,F.P. (2006) Interaction of carcinogen-bound DNA with individual DNA polymerases. *Chem. Reviews*, **106**, 420–452.
62. Lehman,A.R. (2006) Clubbing together on clamps: the key to translesion synthesis. *DNA Repair*, **5**, 404–407.